Acta Cryst. (1980). A**36**, 520–530

X-ray Diffraction Study of $Zr(Ca,Y)O_{2-x}$. II. Local Ionic Arrangements

BY M. MORINAGA* AND J. B. COHEN

Department of Materials Science and Engineering, The Technological Institute, Northwestern University, Evanston, Illinois 60201, *USA*

AND J. FABER JR

Materials Science Division, Argonne National Laboratory, Argonne, Illinois 60201, *USA*

(*Received* 26 *October* 1979; *accepted* 29 *January* 1980)

Abstract

Above the 1300 K transition and in the defect fluorite phase, there is diffuse X-ray scattering which is similar for both Ca- and Y-stabilized zirconias. This is largely due to ionic displacements from the average structure, principally oxygen ions displaced locally in ⟨100⟩ directions. It has been proposed that some of this scattering is due to fine precipitates of $ZrCa_4O_9$ or ZrY_4O_9. The quantitative analysis of this diffuse scattering reported here does indeed indicate some similarities to this phase; in particular the stabilizing ions form rods in the $\langle\bar{3}\bar{3}2\rangle$ directions similar to those in the precipitate. However, in this compound the stabilizing ion is a second neighbor to an oxygen-ion vacancy, whereas the present results indicate that these tend to be first neighbors. This is the first direct evidence for this association in these materials. This probably occurs to reduce local distortions and to provide local charge balance. It is concluded that the diffuse intensity is from locally ordered regions, not precipitates.

Introduction

Calcia- and yttria-stabilized zirconias are well known solid electrolytes that exhibit fast anion conduction above 1300 K. In the stabilized cubic phase field, both materials have the fluorite structure (Etsell & Flengas, 1970; Roth, 1975). The high ionic conductivity is clearly related to the creation of oxygen vacancies. (The substitutional addition of Ca^{2+} or Y^{3+} for Zr^{4+} produces oxygen vacancies to maintain charge neutrality.) In contrast to the stabilized phases, pure ZrO_2 exhibits the cubic fluorite structure only above 2600 K. Below this temperature, ZrO_2 transforms to a tetragonal phase (Teufer, 1962; Smith & Newkirk, 1965).

For stabilized zirconia, there currently seem to be two different interpretations of the transformation at 1300 K. Either cooperative displacements of the oxygen ions take place, or the ordering of cations, anions and vacancies (Carter & Roth, 1963; Steele & Fender, 1974; Allpress & Rossell, 1975; Allpress, Rossell & Scott, 1975; Hudson & Moseley, 1976, 1978; Faber, Mueller & Cooper, 1978).

Employing primarily neutron diffraction with powders of $Zr(Ca)O_{2-x}$, Carter & Roth (1963, 1968) concluded that even in the disordered state of stabilized zirconias there are displacements of the oxygen ions (0·2–0·3 Å) from the ideal positions in the fluorite structure; these were reported to be in ⟨111⟩ directions and the authors inferred that the 1300 K transition was due to the establishment of cooperative long-range motions in these directions. However, Steel & Fender (1974) (with similar procedures) reported oxygen displacements in ⟨100⟩ directions in disordered $Zr(Y)O_{2-x}$. Employing neutrons and single crystals, Faber, Mueller & Cooper (1978) found that in the ordered phase of *both* Ca- and Y- stabilized zirconias the oxygen ions were displaced periodically in ⟨100⟩ directions. In part I of this study (Morinaga, Cohen & Faber, 1979), X-rays and single-crystals were employed and oxygen-ion displacements in ⟨100⟩ directions were found in *both* materials, even above the 1300 K transition. These are of the same magnitude as those associated with the cubic to tetragonal transition at 2600 K in pure ZrO_2 (Teufer, 1962; Smith & Newkirk, 1965).

However, the 1300 K transition in the stabilized zirconias is quite sluggish and therefore clearly involves the cations, whose diffusivities are five orders of magnitude lower than those for the anions (Estell & Flengas, 1970). In fact, based on the location of (diffuse) scattering in electron diffraction patterns (in

* Present address: Toyohashi University of Technology, Toyohashi-shi, Aichi 440, Japan.

0567-7394/80/040520-11$01.00

addition to the spots from the fluorite phase), Allpress & Rossell (1975) and Allpress, Rossell & Scott (1975) suggest that domains of $CaZr_4O_9$ approximately 30 Å in size are embedded in the matrix of the disordered state of the calcia-stabilized zirconias. For this analysis, its structure was assumed to be that of $CaHf_4O_9$, as the corresponding Zr phase has not yet been studied in bulk form. In fact, Carter & Roth (1963, 1968) had earlier suggested some small precipitate as one possible source of some of the diffuse scattering observed in their study of the disordered phase.

In this investigation, quantitative measurements have been made of the diffuse X-ray intensity scattered by single crystals of disordered Ca- and Y-stabilized zirconia. Short-range-order parameters and displacements have been evaluated, and from these both the ionic arrangements and displacements in the disordered phase have been clarified.

Experimental procedures

Materials

The growth and analysis of the $Zr_{0.850}Ca_{0.150}O_{1.850}$ and $Zr_{0.786}Y_{0.214}O_{1.893}$ crystals are described in part I. After holding them in air at 1673 K for 2·5 h, they were cooled rapidly by turning off power to the furnace. At 1523 K they were removed from the furnace to increase the cooling rate and preserve the disordered state (see part I for checks of this fact). These crystals had plate-like geometry and were larger than the X-ray beam.

Diffraction techniques

The crystals were held in a vacuum attachment to a GE quarter-circle goniostat (at 1·3–2·7 Pa); the cover was a thin Be hemisphere. Measurements were carried out on an automated GE XRD-5 diffractometer (Schwartz, Morrison & Cohen, 1963) which was equipped with adjustable receiving and scatter slits for the diffracted beam. The incident beam was Cu $K\alpha$ radiation (40 kV, 20 mA) from a pyrolytic graphite monochromator bent to focus in the vertical direction at the receiving slit. The beam divergences obtained by measurement of a 200 Bragg reflection from a cleaved LiF crystal, were $\Delta h_{\text{horizontal}} = 0{\cdot}06$ and $\Delta h_{\text{vertical}} = 0{\cdot}08$ r.l.u.

For $Zr(Y)O_{2-x}$, intensities were measured with a scintillation detector equipped with a pulse-height analyzer (set to accept 90% of the Cu $K\alpha$). Balanced filters of Ni and Co were also employed (Morinaga & Cohen, 1979) to minimize contributions from fluorescence and the $\lambda/2$ component. With $Zr(Ca)O_{2-x}$, an intrinsic Ge detector was used with a 500 eV window (which reduced the measurement time).

The 4–5% variation of beam intensity over the measuring times of 3–4 weeks for each crystal was monitored and corrected by making counts *vs* 10^6 counts in a second detector. This monitor channel recorded the fluorescent intensity produced by the incident beam on passing through a thin Co foil before the specimen, which attenuated the beam by approximately 12%. The power of the direct beam, $P_0 = 4{\cdot}0\,(2) \times 10^7$ Hz, was determined by measuring the diffracted intensity from an Al powder briquette (Batterman, Chipman & DeMarco, 1961).

Under the same conditions, the scattering from the air path and electronic noise were measured as a function of scattering angle (2θ) by replacing the specimen with a Pb beam trap. With $Zr(Y)O_{2-x}$ this was 0·06 Hz. The effects of surface roughness were determined following de Wolff (1956). The Zr $K\alpha$ and Y $K\alpha$ produced by Mo $K\alpha$ were measured and normalized to the values at high 2θ. The correction was at most 2% (at 30° 2θ). All data were also corrected for the measured dead time (Schwartz & Cohen, 1977).

Scattering theory

Hayakawa & Cohen (1975) have derived general equations for the diffuse scattering from materials with multiple sublattices, including up to quadratic terms in atomic displacements.

The total coherent diffuse scattering intensity, I_D, in Laue units is given by

$$\begin{aligned} I_D(h)/I_{\text{LM}}(h) = {} & I_{\text{SRO}}(h) \\ & + h_1 Q_x(h) + h_2 Q_Y(h) + h_3 Q_z(h) \\ & + h_1^2 R_x(h) + h_2^2 R_y(h) + h_3^2 R_z(h) \\ & + h_1 h_2 S_{xy}(h) + h_2 h_3 S_{yz}(h) \\ & + h_3 h_1 S_{zx}(h), \end{aligned} \tag{1}$$

where $h = (h_1,h_2,h_3)$ and h_1, h_2 and h_3 are continuous variables in reciprocal space. The term I_{LM} is the Laue monotonic scattering due to a random array of defects without displacements.

In (1), the first term on the right-hand side is the short-range-order intensity [$I_{\text{SRO}}(h)$], the next three terms are the size-effect scattering due to average interatomic displacements (whose components are in a direction indicated by the subscript) and the remaining terms are the first-order thermal diffuse scattering (TDS) plus Huang (1947) scattering, due to mean-square static displacements).

$$I_{\text{SRO}}(h) = \sum_l \sum_m \sum_n \bar{\alpha}_{lmn} \cos 2\pi(h_1 l + h_2 m + h_3 n), \tag{2a}$$

$$Q_x(h) = -\sum_l \sum_m \sum_n \bar{\gamma}^x_{lmn} \sin 2\pi(h_1 l + h_2 m + h_3 n), \tag{2b}$$

$$R_x(h) = \sum_l \sum_m \sum_n \bar{\delta}^x_{lmn} \cos 2\pi(h_1 l + h_2 m + h_3 n), \quad (2c)$$

$$S_{xy}(h) = \sum_l \sum_m \sum_n \bar{\varepsilon}^{xy}_{lmn} \cos 2\pi(h_1 l + h_2 m + h_3 n), \quad (2d)$$

with similar definitions for $Q_y(h)$, $R_y(h)$, $S_{yz}(h)$, $Q_z(h)$, $R_z(h)$ and $S_{zx}(h)$. The $\langle lmn \rangle$ are interatomic vectors defined by

$$\mathbf{r}_{lmn} = l\mathbf{a}_1 + m\mathbf{a}_2 + n\mathbf{a}_3, \quad (3a)$$

where $\mathbf{a}_1$, $\mathbf{a}_2$ and $\mathbf{a}_3$ are the usual cubic axes in real space. The diffraction vector $\mathbf{k}$ is given in terms of the axes $\mathbf{b}_i$ in reciprocal space:

$$\mathbf{k} = 2\pi(\mathbf{S} - \mathbf{S}_0)/\lambda = 2\pi(h_1\mathbf{b}_1 + h_2\mathbf{b}_2 + h_3\mathbf{b}_3), \quad (3b)$$

where $\mathbf{S}$ and $\mathbf{S}_0$ are unit vectors in the directions of the scattered and incident beams, respectively, and λ is the wavelength of X-rays.

The coefficients in the series (2) are weighted averages of vectors spanning different sublattices. For example, the short-range-order parameters $\bar{\alpha}_{lmn}$ are made up of terms involving

$$\alpha^{ij}_{\mu\nu}(lmn) = 1 - P^{ij}_{\mu\nu}/x^j_\nu, \quad (4)$$

x^j_ν denotes the sublattice fraction of the jth component on the νth sublattice, and $P^{ij}_{\mu\nu}$ is the conditional probability of finding j-type atoms on the νth sublattice, separated by vector $\mathbf{r}_{lmn}$ from an i atom on the μth sublattice. The fluorite structure is shown in Fig. 1. The various sublattices in $Zr(Ca)O_{2-x}$ and $Zr(Y)O_{2-x}$ are given in Table 1. For $m3m$ symmetry, sites labelled tetrahedral 1 and 2 are equivalent. The f.c.c. sites (F) are occupied by cations [Zr and Ca (or Y)] with oxygen ions in tetrahedral sites. The tetrahedral sites are indicated by a T. The three types of interatomic vectors are given in Table 2, which also illustrates the sublattices that are spanned for each type of vector. With these tables and the known concentrations of defects, the equations for the coefficients in (2) can be readily derived following Hayakawa & Cohen (1975) and are summarized in Tables 3 and 4.

The X, Y, Z refer to the components of the interatomic displacements from average sites of species i on μ, j on ν. Thus,

$$\bar{\gamma}^x_{lmn} \propto \langle X^{ij}_{\mu\nu} \rangle, \quad (5a)$$

$$\bar{\delta}^x_{lmn} \propto \langle X^i_\mu X^j_\nu \rangle, \quad (5b)$$

$$\bar{\varepsilon}^{xy}_{lmn} \propto \langle X^i_\mu Y^j_\nu \rangle. \quad (5c)$$

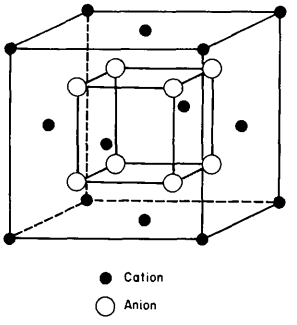

Fig. 1. The fluorite structure.

Table 2. *The three types of interatomic vectors and the corresponding sublattice pairs for the fluorite structure*

Type of *lmn*	Possible sublattice pairs
1. *l,m,n* all [2*p*]/4 $l + m + n = [4q]/4$	f.c.c.–f.c.c., tet 1–tet 1, tet 2–tet 2
2. *l,m,n* all [2*p*]/4 $l + m + n = [4q + 2]/4$	tet 1–tet 2, tet 2–tet 1
3. *l,m,n* [2*p* + 1]/4	f.c.c.–tet 1, f.c.c.–tet 2, tet 1–f.c.c., tet 2–f.c.c.

Table 3. *Laue monotonic scattering and $\bar{\alpha}_{lmn}$ for the fluorite structure*

The scattering factors f_i in this table include the temperature factors, which were taken from part I of this study. M = Zr, N = Ca(Y).

Laue monotonic $\quad x^M_F x^N_F (f_M - f_N)^2 + 2x^O_T x^{V_O}_T f^2_O$

$\bar{\alpha}_{lmn}$:

Type 1 $\quad \dfrac{x^M_F x^N_F (f_M - f_N)^2 \alpha^{MN}_{FF} + 2x^O_T x^{V_O}_T f^2_O \alpha^{OV_O}_{TT}}{x^M_F x^N_F (f_M - f_N)^2 + 2x^O_T x^{V_O}_T f^2_O}$

Type 2 $\quad \dfrac{2x^O_T x^{V_O}_T f^2_O \alpha^{OV_O}_{TT}}{x^M_F x^N_F (f_M - f_N)^2 + 2x^O_T x^{V_O}_T f^2_O}$

Type 3 $\quad \dfrac{4f_O(f_M - f_N) x^M_F x^{V_O}_T \alpha^{MV_O}_{FT}}{x^M_F x^N_F (f_M - f_N)^2 + 2x^O_T x^{V_O}_T f^2_O}$

Table 1. *Sublattice fractions and sublattice vectors for the fluorite structure*

$Zr_{0.850}Ca_{0.150}O_{1.850}$; $a = 0.150$, $b = 0.075$. $Zr_{0.786}Ca_{0.214}O_{1.893}$; $a = 0.214$, $b = 0.0535$.

Type of sublattice	Sublattice vector	Sublattice fractions M = Zr	N = Ca(Y)	O	Vacancy
f.c.c.	0,0,0	$x^M_F = 1 - a$	$x^N_F = a$	$x^O_F = 0$	$x^{V_O}_F = 0$
Tetrahedral 1	1/4,1/4,1/4	$x^M_{T_1} = 0$	$x^N_{T_1} = 0$	$x^O_{T_1} = 1 - b$	$x^{V_O}_{T_1} = b$
Tetrahedral 2	3/4,3/4,3/4	$x^M_{T_2} = 0$	$x^N_{T_2} = 0$	$x^O_{T_2} = 1 - b$	$x^{V_O}_{T_2} = b$

Here, $X^{ij}_{\mu\nu} = X^i_\mu - X^j_\nu$, where X^i_μ is the displacement along the x direction of the ith atom on the μth sublattice.

The parameters $\bar{\alpha}$, $\bar{\gamma}$, $\bar{\delta}$, $\bar{\varepsilon}$ were determined by a least-squares fit to (1) (Williams, 1972). This method is especially suitable for systems with more than one sublattice, as in this study. Separating the various components by their different symmetries (Borie & Sparks, 1971) requires large volumes in reciprocal space (*e.g.* Hayakawa & Cohen, 1975) and in such volumes the variations in the scattering-factor terms in Tables 3 and 4 are not sufficiently small to utilize this procedure. The least-squares procedure has been used successfully in previous studies of oxides (Terauchi & Cohen, 1979; Morinaga & Cohen, 1979). The region of measurement in this study is illustrated in Fig. 2. This volume was chosen to be as compact as possible to minimize variation in the scattering factors, and to avoid $2\theta < 30°$, where the beam was larger than the specimen.

Data were obtained at intervals $\Delta h = 0{\cdot}1$, the total number of points actually sampled being 3100 for $Zr(Y)O_{2-x}$ and 3300 for $Zr(Ca)O_{2-x}$. The number of parameters tried in the fit was 50–110; this will be discussed further with the results.

The atomic scattering factors f_{Zr}, f_{Ca} and f_Y were taken from *International Tables for X-ray Crystallography* (1974) assuming that the ionic states are Zr^{4+}, Ca^{2+} and Y^{3+}. The value of f_O was taken from Tokonami (1965) assuming that the ionic state is O^{2-}. An anomalous dispersion correction for Cu $K\alpha$ radiation was taken into account for all the elements (*International Tables for X-ray Crystallography*, 1974).

The Compton modified scattering was taken from Cromer (1969) and subtracted after correcting for the

Table 4. $\bar{\gamma}^x_{lmn}$, $\bar{\delta}^x_{lmn}$ *and* $\bar{\varepsilon}^{xy}_{lmn}$ *for the fluorite structure*

$$L = x_F^M x_F^N (f_M - f_N)^2 + 2x_T^0 x_T^{V^0} f_O^2;\ M = \mathrm{Zr},\ N = \mathrm{Ca(Y)}.$$

The scattering factors f_i in this table include temperature factors, taken from part I of this study.

$\bar{\gamma}^x_{lmn}$

Type 1
$$\frac{2\pi}{L}\left[x_F^M f_M^2(x_F^M + x_F^N \alpha_{FF}^{MN})\langle X_{FF}^{MM}\rangle + x_F^N f_N^2(x_F^N + x_F^M \alpha_{FF}^{NM})\langle X_{FF}^{NN}\rangle + 2x_T^0 f_O^2(x_T^0 + x_T^{V^0}\alpha_{TT}^{OV^0})\langle X_{TT}^{OO}\rangle\right]$$

Type 2
$$\frac{2\pi}{L}\left[2x_T^0 f_O^2(x_T^0 + x_T^{V^0}\alpha_{TT}^{OV^0})\langle X_{TT}^{OO}\rangle\right]$$

Type 3
$$0$$

$\bar{\delta}^x_{lmn}$

Type 1
$$\frac{4\pi^2}{L}\left[x_F^M f_M^2(x_F^M + x_F^N \alpha_{FF}^{MN})\langle X_F^M X_F^M\rangle + x_F^N f_N^2(x_F^N + x_F^M \alpha_{FF}^{NM})\langle X_F^N X_F^N\rangle + 2x_T^0 f_O^2(x_T^0 + x_T^{V^0}\alpha_{TT}^{OV^0})\langle X_T^0 X_T^0\rangle\right.$$
$$\left. + x_F^M x_F^N f_M f_N(1 - \alpha_{FF}^{MN})\langle X_F^M X_F^N\rangle + x_F^N x_F^M f_M f_N(1 - \alpha_{FF}^{NM})\langle X_F^N X_F^N\rangle\right]$$

Type 2
$$\frac{8\pi^2}{L}\left[x_T^0 f_O^2(x_T^0 + x_T^{V^0}\alpha_{TT}^{OV^0})\langle X_T^0 X_T^0\rangle\right]$$

Type 3
$$\frac{8\pi^2}{L}\left[x_F^M x_T^0 f_M f_O(1 - \alpha_{FT}^{MO})\langle X_F^M X_T^0\rangle + x_F^N x_T^0 f_N f_O(1 - \alpha_{FT}^{NO})\langle X_F^N X_T^0\rangle + x_T^0 x_F^M f_O f_M(1 - \alpha_{TF}^{OM})\langle X_T^0 X_F^M\rangle\right.$$
$$\left. + x_T^0 x_F^N f_O f_N(1 - \alpha_{TF}^{ON})\langle X_T^0 X_F^N\rangle\right]$$

$\bar{\varepsilon}^{xy}_{lmn}$

Type 1
$$\frac{8\pi^2}{L}\left[x_F^M f_M^2(x_F^M + x_F^N \alpha_{FF}^{MN})\langle X_F^M Y_F^N\rangle + x_F^N f_N^2(x_F^N + x_F^M \alpha_{FF}^{NM})\langle X_F^N Y_F^N\rangle + 2x_T^0 f_O^2(x_T^0 + x_T^{V^0}\alpha_{TT}^{OV^0})\langle X_T^0 Y_T^0\rangle\right.$$
$$\left. + x_F^M x_F^N f_M f_N(1 - \alpha_{FF}^{MN})\langle X_F^M Y_F^N\rangle + x_F^N x_F^M f_M f_N(1 - \alpha_{FF}^{NM})\langle X_F^N Y_F^M\rangle\right]$$

Type 2
$$\frac{16\pi^2}{L}\left[x_T^0 f_O^2(x_T^0 + x_T^{V^0}\alpha_{TT}^{OV^0})\langle X_T^0 Y_T^0\rangle\right]$$

Type 3
$$\frac{16\pi^2}{L}\left[x_F^M x_T^0 f_M f_O(1 - \alpha_{FT}^{MO})\langle X_F^M Y_T^0\rangle + x_F^N x_T^0 f_N f_O(1 - \alpha_{FT}^{NO})\langle X_F^N Y_T^0\rangle + x_T^0 x_F^M f_O f_M(1 - \alpha_{TF}^{OM})\langle X_T^0 Y_F^M\rangle\right.$$
$$\left. + x_T^0 x_F^N f_O f_N(1 - \alpha_{TF}^{ON})\langle X_T^0 Y_F^N\rangle\right]$$

background, polarization factor, surface roughness and placing the data on an absolute scale. Then, the least-squares procedure was applied.

As the $\bar{\alpha}_{lmn}$ are combinations of several $\alpha_{\mu\nu}^{ij}$ (Table 3), and we really wish to know the Warren short-range-order parameters $\alpha_{\mu\nu}^{ij}$, we next consider which of these $\alpha_{\mu\nu}^{ij}$ can be obtained experimentally.

(i) $Zr(Ca)O_{2-x}$ [$x_F^N = 15{\cdot}0\%$ (N = Ca, M = Zr) *and* $x_T^{V_O} = 7{\cdot}5\%$]

(*a*) *Type* 1 *vectors.* The $\bar{\alpha}_{lmn}$ are combinations of α_{FF}^{MN} and $\alpha_{TT}^{OV_O}$. The diffuse scattering was measured in the range $0{\cdot}146 < \sin\theta/\lambda < 0{\cdot}476$. Therefore, the $\bar{\alpha}_{lmn}$ can be written

$$\bar{\alpha}_{lmn} \simeq 0{\cdot}947\,\alpha_{FF}^{MN} + 0{\cdot}053\,\alpha_{TT}^{OV_O},$$
$$\therefore \bar{\alpha}_{lmn} \simeq \alpha_{FF}^{MN}, \tag{6}$$

for the present measurements (the values of f_O, f_{Zr} and f_{Ca} were those at $\sin\theta/\lambda = 0{\cdot}311$, the center of the measured regions). Thus, α_{FF}^{MN} can be determined from the measured $\bar{\alpha}_{lmn}$, because the contribution of $\alpha_{TT}^{OV_O}$ to $\bar{\alpha}_{lmn}$ is negligibly small. Also, the Laue monotonic scattering $I_{LM} = x_F^M x_F^N (f_M - f_N)^2 + 2x_T^O x_T^{V_O} f_O^2 \simeq 28{\cdot}81$.

(*b*) *Type* 2 *vectors.*

$$\bar{\alpha}_{lmn} \simeq 0{\cdot}053\,\alpha_{TT}^{OV_O}. \tag{7}$$

Compared to α_{FF}^{MN} for type 1 vectors the contribution of $\alpha_{TT}^{OV_O}$ is small and it is difficult to determine it accurately.

(*c*) *Type* 3 *vectors.*

$$\alpha_{FT}^{MV_O} \simeq 2{\cdot}33\,\bar{\alpha}_{lmn}. \tag{8}$$

Thus, $\alpha_{FT}^{MV_O}$ can be determined from the measured $\bar{\alpha}_{lmn}$.

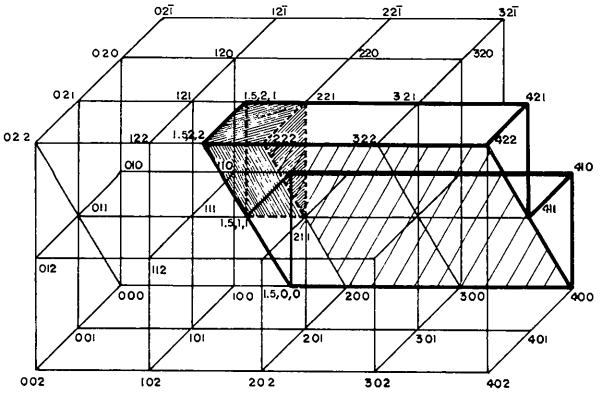

Fig. 2. Measurements were carried out in the region indicated by dark lines. The small region with fine shading was measured for $Zr(Ca)O_{2-x}$, but not for $Zr(Y)O_{2-x}$. (The measured intensity in the area with coarse shading is shown in Fig. 3.)

(ii) $Zr(Y)O_{2-x}$ [$x_F^N = 21{\cdot}4\%$ (N = Y, M = Zr) *and* $x_T^{V_O} = 5{\cdot}35\%$]

$$I_{LM} = x_F^M x_F^N (f_M - f_N)^2 + 2x_T^O x_T^{V_O} f_O^2 \simeq 1{\cdot}20.$$

[The value of the Laue monotonic scattering for $Zr(Y)O_{2-x}$ is actually smaller by a factor of 24 than that for $Zr(Ca)O_{2-x}$ because $f_{Zr} \simeq f_Y$.]

(*a*) *Type* 1 *vectors.*

$$\bar{\alpha}_{lmn} = 0{\cdot}064\,\alpha_{FF}^{MN} + 0{\cdot}936\,\alpha_{TT}^{OV_O}$$
$$\simeq \alpha_{TT}^{OV_O}. \tag{9}$$

(*b*) *Type* 2 *vectors.*

$$\bar{\alpha}_{lmn} \simeq 0{\cdot}936\,\alpha_{TT}^{OV_O} \simeq \alpha_{TT}^{OV_O}. \tag{10}$$

(*c*) *Type* 3 *vectors.*

$$\alpha_{FT}^{MV_O} \simeq 3{\cdot}18\,\bar{\alpha}_{lmn}. \tag{11}$$

The $CaZr_4O_9$ phase proposed to cause the diffuse scattering by Allpress, Rossell & Scott (1975) involves primarily cation ordering on the f.c.c. sublattice, and hence we can examine this model with the values of α_{FF}^{MN} for $Zr(Ca)O_{2-x}$.

It is also worth noting (see Table 4) that the displacement terms for type 2 vectors arise *only* from the oxygen ion–oxygen ion interactions. Thus the various proposed models for displacements can also be examined.

Results and discussion

Qualitative features of the diffuse scattering

The observed total diffuse scattering in Laue units per atom (*i.e.* divided by the Laue intensity) for both zirconias is shown in Fig. 3. Because the Laue monotonic scattering for $Zr(Y)O_{2-x}$ is so small compared to that for $Zr(Ca)O_{2-x}$, the intensities shown in Fig. 3 are much larger for the Y case than for the Ca-stabilized phase. This fact also implies that the contribution of local order to the total intensity is small, since the total amount of such scattering is the Laue monotonic term [$I_{SRO}(h)$ in (1)].

The positions of the diffuse peaks are similar for both oxides. We consider now the interpretation by Allpress & Rossell (1975) that this scattering is due to small precipitates. One similar structure is that of $CaHf_4O_9$ (Allpress, Rossell & Scott, 1975). Its space group is $C\,2/c$, $a = 17{\cdot}698\ (2)$, $b = 14{\cdot}500\ (1)$, $c = 12{\cdot}021\ (1)$ Å, $\beta = 119{\cdot}468\ (6)°$. The proposed relationship to the fluorite structure (f) is $a = [222]_f$, $b = [\bar{2}20]_f$, $c = \frac{1}{2}[\bar{3}\bar{3}2]_f$. The unit cell contains 80 cations and 144 anions. Assuming that this is like the local structure in both the oxides studied here, and that all orientations of these regions are possible, then b can be parallel to any

of the twelve directions in the fluorite form ⟨110⟩, and the observed pattern should be a superposition of all such orientations, each with equal probability. The calculated $|F|^2$ values on the ($hh0$) plane in reciprocal space are shown in Fig. 4. In the assumed structure ($CaHf_4O_9$) there are displacements of cations from the fluorite positions. The values in Fig. 4 in parentheses are the calculated intensities *without* these displacements. By comparing Figs. 3 and 4 it can be seen that: (i) the calculated intensities do not agree well with the measurements, for both the Ca- and Y-stabilized zirconias; (ii) if there are small precipitates like $CaHf_4O_9$, several strong peaks are missing from the measurements. Also, at least for $Zr(Y)O_{2-x}$, the calculated intensities are sensitive to the actual displacements.

The structure of the Hf phase is not well established as only powder data at modest angles were applied in the published analysis, and the R value was poor. [Allpress, Rossell & Scott (1975) report a low value, but the intensities presented in their paper give $R \simeq 0{\cdot}5$.] But with the limits of the information available, the diffuse scattering does not appear to be due to small precipitates like this phase.

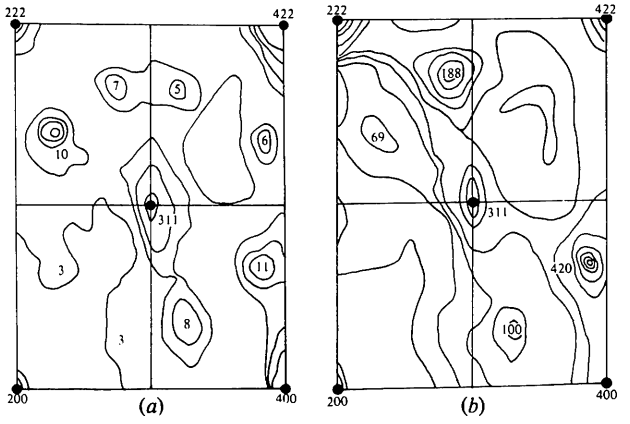

Fig. 3. Observed total diffuse intensity in Laue units per atom [$I_D(h)/I_{LM}$ in equation (1)]. Filled circles are fluorite reflections. (*a*) $Zr(Ca)O_{2-x}$; (*b*) $Zr(Y)O_{2-x}$.

Quantitative results

(i) *Short-range order in* $Zr(Ca)O_{2-x}$

(*a*) *Least-squares analysis.* The $\bar{\alpha}_{lmn}$ from the least-squares analyses are shown in Fig. 5. The number of terms employed in each fit is indicated in parentheses. All weightings were taken as unity. Where indicated, the variations in scattering factors in the terms in Tables 3 and 4 were taken into account with polynomials (see Morinaga, 1978).

The number of $\bar{\alpha}_{lmn}$ was varied from 6–11 for type 1 vectors, 6–9 for type 2 and 5–11 for type 3. This range was established by examining a calculated partial Patterson map for $CaZr_4O_9$ and including in the least-squares analysis all significant interatomic vectors.

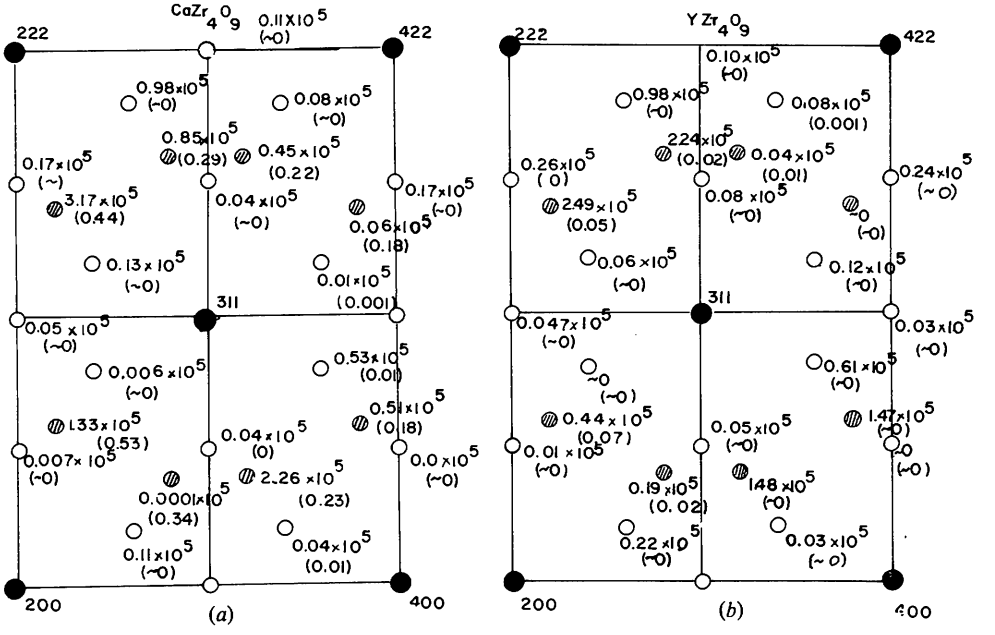

Fig. 4. Calculated intensities ($|F|^2$) due to all possible orientations of a precipitate '$CaZr_4O_9$' in (*a*) or 'YZr_4O_9' in (*b*). ●: fluorite peaks; ◍: observed diffuse scattering; ○: other reflections that should arise from these precipitates. Numbers in parentheses are the calculated intensities ($\times 10^5$) without the atomic displacements in $CaHf_4O_9$. Other numbers include these displacements.

Note in Fig. 5 that only $\bar{\alpha}_{\frac{1}{4}[220]}$ and $\bar{\alpha}_{\frac{1}{4}[400]}$ (for type 1 vectors) are sensitive to the number of parameters employed in the fit. The others are quite stable.

(b) Further comparison to the proposed $CaZr_4O_9$ *phase.* The $\bar{\alpha}_{lmn}$ for the model for $ZaZr_4O_9$ suggested by Allpress, Rossell & Scott (1975) were obtained from a partial Patterson synthesis (superstructure reflections only). The volumes of the peaks are directly related to these α's (Koch & Cohen, 1969). These $\bar{\alpha}$'s are shown in Fig. 6. While the magnitudes are much larger, the pattern is quite similar to that in Fig. 5.

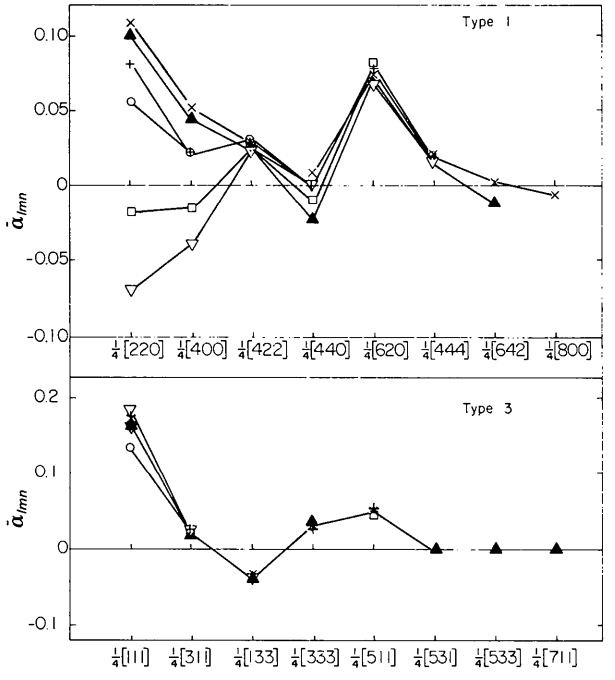

Fig. 5. Short-range order parameters α_{lmn} *vs lmn* for $Zr(Ca)O_{2-x}$. The number of terms of each type in the least-squares fit to the intensity is given in parentheses. The R value is the overall fit to the measured intensity.

(1) ×: $\bar{\alpha}_0$, $\bar{\alpha}(22)$, $\bar{\gamma}(30)$, $\bar{\delta}_0$, $(\bar{\delta}+\bar{\varepsilon})(56) = 110$; $\bar{\alpha}_{000} = 1{\cdot}58$, $R = 15{\cdot}6\%$.
(2) ▲: $\bar{\alpha}_0$, $\bar{\alpha}(17)$, $\bar{\gamma}(24)$, $\bar{\delta}_0$, $(\bar{\delta}+\bar{\varepsilon})(52) = 95$; $\bar{\alpha}_{000} = 1{\cdot}54$, $R = 16{\cdot}2\%$.
(3) +: $\bar{\alpha}_0$, $\bar{\alpha}(11)$, $\bar{\gamma}(17)$, $\bar{\delta}_0$, $(\bar{\delta}+\bar{\varepsilon})(36) = 66$; $\bar{\alpha}_{000} = 1{\cdot}47$, $R = 16{\cdot}9\%$.
(4) O: $\bar{\alpha}_0$, $\bar{\alpha}(11)$, $\bar{\gamma}(17)$, $\bar{\delta}_0$, $(\bar{\delta}+\bar{\varepsilon})(37) = 67$; $\bar{\alpha}_{000} = 1{\cdot}38$, $R = 16{\cdot}9\%$.
(5) □: $\bar{\alpha}_0$, $\bar{\alpha}(17)$, $\bar{\gamma}(17)$, $\bar{\delta}_0$, $(\bar{\delta}+\bar{\varepsilon})(36) = 72$; $\bar{\alpha}_{000} = 1{\cdot}40$, $R = 16{\cdot}4\%$.
(6) ▽: $\bar{\alpha}_0$, $\bar{\alpha}(17)$, $\bar{\gamma}(17)$, $\bar{\delta}_0$, $(\bar{\delta}+\bar{\varepsilon})(36) = 72$; $\bar{\alpha}_{000} = 1{\cdot}48$; $R = 16{\cdot}0\%$.

For runs (1)–(4), the short-range-order parameters for type 2 vectors were not included, but these were included for runs (5) and (6). (All the $\bar{\alpha}_{lmn} < 0{\cdot}1$ for type 2 vectors.) The difference between (5) and (6) is due to the polynomial fit for the ratios of scattering factors; for run (5), all $\bar{\alpha}$, $\bar{\gamma}$, $\bar{\delta}$ and $\bar{\varepsilon}$ were so fitted, but for run (6) this was done only for the $\bar{\alpha}$'s. A comparison of runs (5) and (6) for $\bar{\gamma}$, $\bar{\delta}$ and $\bar{\varepsilon}$ does not reveal any significant differences. For analyses numbered (1) to (4), this polynomial fitting was employed for all coefficients.

The observed $\alpha_{\frac{1}{4}[111]}$ for type 3 vectors in Fig. 5 is significantly large. According to Table 3, this implies that $\alpha_{FT}^{ZrV_O}(\frac{1}{4}\frac{1}{4}\frac{1}{4}) > 0$, or [from (4)] that $P_{FT}^{ZrV_O} < X_T^{V_O}$. Now, from (4),

$$X_T^{V_O}(1-\alpha_{FT}^{ZrV_O}) = P_{FT}^{ZrV_O}, \tag{12a}$$

$$X_F^{Zr}(1-\alpha_{TF}^{V_OZr}) = P_{TF}^{V_OZr}. \tag{12b}$$

Also,

$$X_F^{Zr}\,P_{FT}^{ZrV_O} = X_T^{V_O}\,P_{TF}^{V_OZr}, \tag{13}$$

and with (12),

$$\alpha_{FT}^{ZrV_O} = \alpha_{TF}^{V_OZr}. \tag{14}$$

Similarly, with N = Ca,

$$\alpha_{FT}^{CaV_O} = \alpha_{TF}^{V_OCa} \tag{15}$$

and

$$X_F^{Ca}(1-\alpha_{TF}^{V_OCa}) = P_{TF}^{V_OCa}. \tag{16}$$

Adding (12*b*) and (16), we get

$$X_F^{Zr}\,\alpha_{TF}^{V_OZr} + X_F^{Ca}\,\alpha_{TF}^{V_OCa} = 0. \tag{17}$$

Substituting (14) and (15), we find

$$\alpha_{FT}^{CaV_O} = -\frac{X_F^{Zr}}{X_F^{Ca}}\,\alpha_{FT}^{ZrV_O}. \tag{18}$$

Therefore, $P_{FT}^{CaV_O} > X_T^{V_O}$. This implies that there is a tendency for Ca^{2+} ions to be surrounded by first-neighbor oxygen vacancies. This result is quite different from the model by Allpress, Rossell & Scott (1975); that model is illustrated in Fig. 7, and in it vacancies are *second* neighbours to a Ca ion (*lmn* = ¼[113]). This near-neighbor pairing of Ca^{2+} and (the effectively positive) oxygen vacancies may arise to reduce the strain energy of the larger Ca ion, or to achieve local charge neutrality since Ca^{2+} replaces Zr^{4+}.

To obtain more information about the chemical arrangements associated with the local order, computer

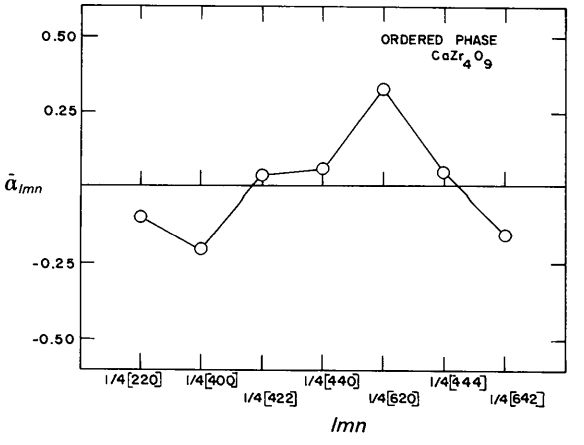

Fig. 6. $\bar{\alpha}_{lmn}$ for $CaZr_4O_9$ calculated from a partial Patterson synthesis of the model suggested by Allpress, Rossell & Scott (1975).

simulations were carried out, employing the method of Gehlen & Cohen, as modifed by Gragg (see Gragg, Bardhan & Cohen, 1971). There were 32 000 cations in the model, 20 × 20 × 20 f.c.c. cells, with periodic boundary conditions. Beginning with a near-random configuration for which $\alpha_l = 0$ for i = 1–6 type 1 vectors to within 1%, the local order was adjusted by the program to satisfy the measured α_l, i = 2–6 to within 2% for type 1 vectors. From (6), these α's relate to the interaction between Zr^{4+} and Ca^{2+}. The resultant structure was then examined on $(1\bar{1}0)$-type planes. On these planes through the $ZrCa_4O_9$ phase, Ca^{2+} ions are predominantly aligned along traces of $[\bar{3}\bar{3}2]$ directions. The short-range order in the fluorite phase clearly manifests itself with more alignments like this than in the random arrangement; compare the circled regions in Figs. 8(*a*) and (*b*).

(*c*) *Synthesis of the intensity.* The various components of the intensity in (1) are presented in Fig. 9, synthesized from the least-squares result. Comparing the total, Fig. 9(*d*), with the total of the size-effect terms alone we find that ~70% of the intensity is due to atomic displacements, 30% due to short-range order.

(ii) *Displacements in* $Zr(Y)O_{2-x}$ *and* $Zr(Ca)O_{2-x}$

For $Zr(Y)O_{2-x}$, the $\bar{\alpha}_{lmn}$ could not be determined. The observed diffuse intensity in Laue units is so large that most of it must be due to size effect, certainly much more so than for $Zr(Ca)O_{2-x}$, where these contributions are already dominant.

The intensities for the Y-stabilized zirconia were therefore analyzed assuming all $\bar{\alpha}_{lmn} = 0$. The synthesized intensities are compared to the measured values in Fig. 10. In Fig. 11 the various coefficients of the displacement terms ($\bar{\gamma}$, $\bar{\delta}$, $\bar{\varepsilon}$) are given for both oxides. The changes with *lmn* are quite similar, except for $\bar{\gamma}$, type 1 vectors. Note that $\bar{\gamma}^x$ and $\bar{\delta}^x$ for *lmn* = $\frac{1}{4}$[200], $\frac{1}{4}$[400] and $\frac{1}{4}$[600] are high. These coefficients are related to ⟨100⟩-type displacements; this result is confirmation of the finding in part I, with the Bragg peaks, that such oxygen-ion displacements are present in the fluorite phase prior to transformation, not the ⟨111⟩-type displacements suggested by Carter & Roth (1963, 1968). As a further test, we note that for ⟨111⟩-type displacements $|\Delta X| = |\Delta Y| = |\Delta Z|$. Therefore, $|\langle \Delta X \Delta X \rangle| = |\langle \Delta Y \Delta Y \rangle| = |\langle \Delta Z \Delta Z \rangle|$. This implies that $|\bar{\delta}^x_{h00}| = |\bar{\delta}^y_{h00}| = |\bar{\delta}^z_{h00}|$, assuming that the oxygen-ion displacements are the dominant terms. The ratios $|\bar{\delta}^y_{h00}/\bar{\delta}^x_{h00}|$ are given in Table 5. It is clear that the Carter & Roth model does not fit the data. On the other hand, the ⟨100⟩ displacements found by Faber, Mueller & Cooper (1978) for the ordered phase are illustrated in Fig. 12. These result in certain conditions for the δ's which are presented in Table 6, and it is clear that these relations are observed from the diffuse scattering in the disordered crystals.

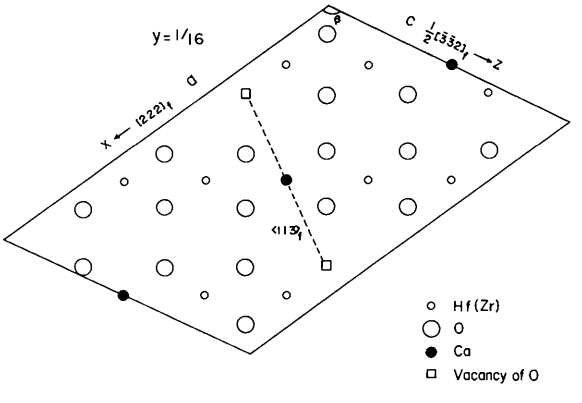

Fig. 7. Section of a model of $CaZr_4O_9$ based on the structure of $CaHf_4O_9$ (Allpress, Rossell & Scott, 1975).

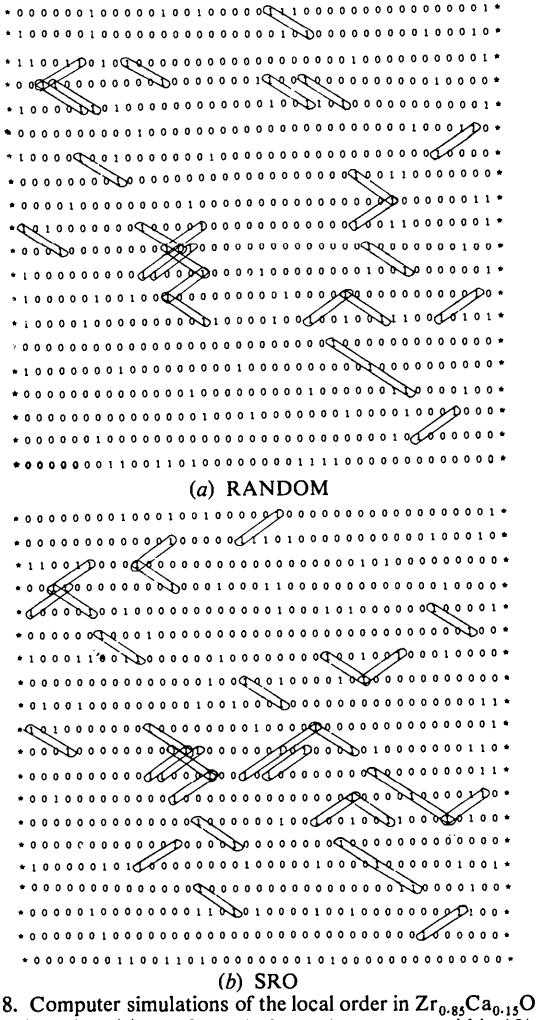

Fig. 8. Computer simulations of the local order in $Zr_{0.85}Ca_{0.15}O_{1.85}$, (110) section. (*a*) $\alpha_l = 0$, i = 1–6 type 1 vectors, to within 1%. (*b*) α_l for i = 2–6 type 1 vectors, which are the average of those in Fig. 5. 1 = Ca^{2+} ions; 0 = Zr^{4+} ions.

Since the type 2 vectors involve only the oxygen-ion displacements (Table 4) it is not necessary to assume that the cations are displaced only small amounts in examining the data for these vectors. The fact that the predictions are born out for type 1 vectors as well, does imply that the cations are displaced very little, as was also found in part I from an analysis of the Bragg peaks.

Table 5. *Measured ratios of* $|\bar{\delta}^y_{h00}/\bar{\delta}^x_{h00}|$

The ranges given include the ranges of the least-square solutions.

	$\lvert\bar{\delta}^y_{\frac{1}{4}[200]}/\bar{\delta}^x_{\frac{1}{4}[200]}\rvert$	$\lvert\bar{\delta}^y_{\frac{1}{4}[400]}/\bar{\delta}^x_{\frac{1}{4}[400]}\rvert$	$\lvert\bar{\delta}^y_{\frac{1}{4}[600]}/\bar{\delta}^x_{\frac{1}{4}[400]}\rvert$
$Zr(Ca)O_{2-x}$	0·2 ~ 1·2	0·3 ~ 1·6	0·2 ~ 0·6
$Zr(Y)O_{2-x}$	0·1	0·1	0·03

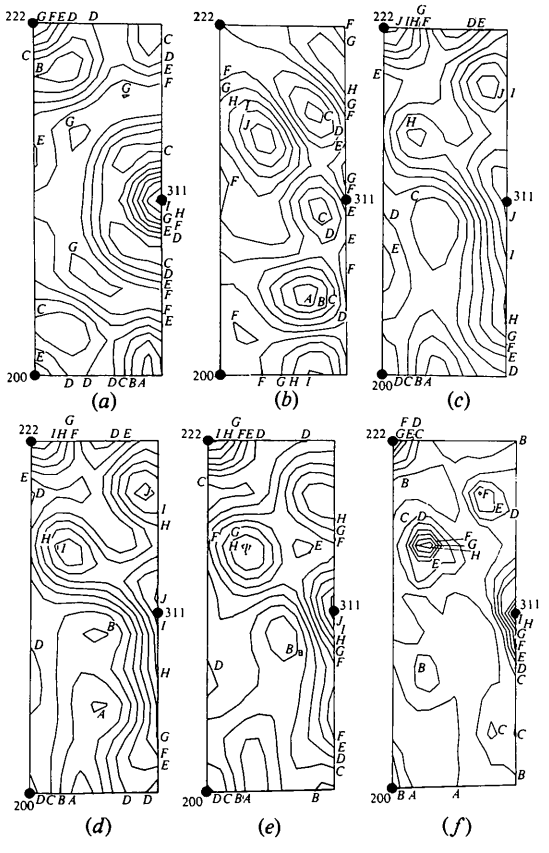

Fig. 9. Components of the diffuse intensity from $Zr(Ca)O_{2-x}$ (in Laue units per atom). Intensity synthesized from the average of the least-squares results. (Filled circles are fluorite reflections.) (*a*) I_{SRO}. Level $A = -0{\cdot}16$, interval = 0·31. (*b*) First-order size-effect scattering [$\sum h_l Q^j$ in equation (1)]. Level $A = -1{\cdot}22$, interval = 0·25. (*c*) TDS + Huang scattering [last six terms in equation (1)]. Level $A = -0{\cdot}50$, interval = 0·48. (*d*) Total size-effect scattering, the sum of (*b*) and (*c*). Level $A = -0{\cdot}38$, interval = 0·47. (*e*) Total synthesized intensity. Level $A = 0{\cdot}50$, interval = 0·68. (*f*) Measured intensity. Level $A = 1{\cdot}265$, interval = 1·13.

Table 6. *Conditions for the model of Faber, Mueller & Cooper* (1978) *and comparison with experimental results*

Vector type	Vector in Fig. 12	Conditions	Followed in data?
Type 2	1	$\bar{\delta}^x_{\frac{1}{4}[200]} = \bar{\delta}^x_{\frac{1}{4}[002]} = \langle \Delta Z \Delta Z \rangle_{\frac{1}{4}[002]} > 0$	yes
	2	$\bar{\delta}^y_{\frac{1}{4}[200]} = \bar{\delta}^x_{\frac{1}{4}[200]} = \bar{\delta}^x_{\frac{1}{4}[020]} = \bar{\delta}^x_{\frac{1}{4}[020]} < 0$	yes
Type 1	3	$\bar{\delta}^x_{\frac{1}{4}[220]} > 0$	yes
	4	$\bar{\delta}^x_{\frac{1}{4}[400]} = \bar{\delta}^x_{\frac{1}{4}[004]} = \langle \Delta Z \Delta Z \rangle_{\frac{1}{4}[004]} > 0$	yes
	5	$\bar{\delta}^y_{\frac{1}{4}[400]} = \bar{\delta}^x_{\frac{1}{4}[400]} = \bar{\delta}^x_{\frac{1}{4}[040]} = \bar{\delta}^x_{\frac{1}{4}[040]} > 0$	no
Type 2	6	$\bar{\delta}^x_{\frac{1}{4}[600]} = \bar{\delta}^x_{\frac{1}{4}[006]} = \langle \Delta Z \Delta Z \rangle_{\frac{1}{4}[006]} > 0$	yes
	7	$\bar{\delta}^y_{\frac{1}{4}[600]} = \bar{\delta}^x_{\frac{1}{4}[600]} = \bar{\delta}^x_{\frac{1}{4}[060]} = \bar{\delta}^x_{\frac{1}{4}[060]} < 0$	depends on particular least-squares solution

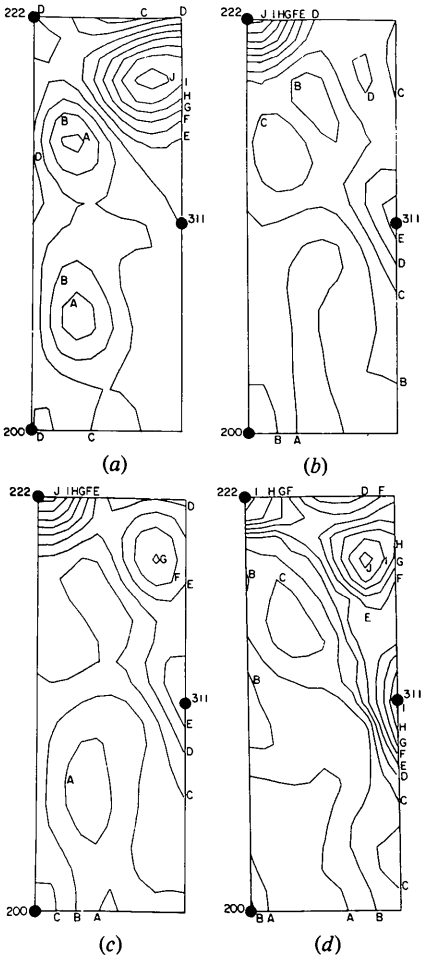

Fig. 10. Components of the diffuse intensity (in Laue units per atom) from $Zr(Y)O_{2-x}$ synthesized from the least-squares result. (*a*) First-order size-effect scattering. Level $A = -33{\cdot}74$, interval = 11·28. (*b*) TDS + Huang scattering. Level $A = 27{\cdot}36$, interval = 28·19. (*c*) (*a*) + (*b*); level $A = 2{\cdot}85$, interval = 30·77. (*d*) Measured intensity. Level $A = 17{\cdot}10$, interval = 17·99. For the least-squares results (with 17 δ terms, $\bar{\delta}_0$ and 36 other $(\bar{\delta} + \bar{\varepsilon})$ terms) $R = 0{\cdot}20$.

The results also suggest that the regions with ⟨100⟩ displacements are quite small. The magnitudes of the γ's, for example, decrease quickly with increasing *lmn*, whereas in the ordered phase these have a periodicity of one fluorite cell. Furthermore, $\gamma^x_{\frac{1}{4}[200]}$ should be zero if the displacements are identical to those below 1300 K as these vectors span the nodes of the oxygen displacement waves. As this is not the case, displacements are much less correlated in the disordered phase.

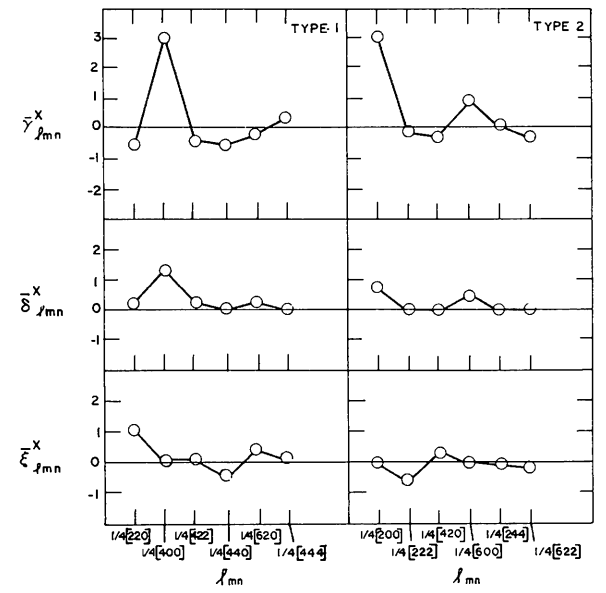

(*a*)

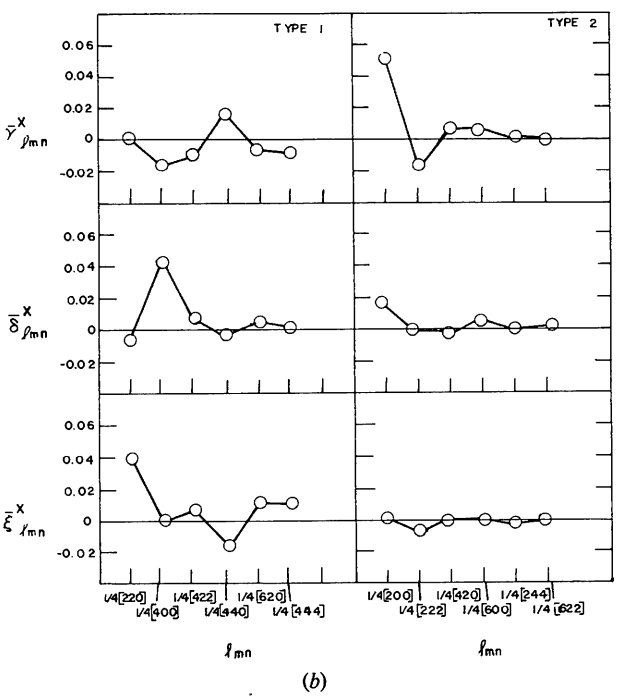

(*b*)

Fig. 11. Coefficients of the displacement terms in equation (1): (*a*) $Zr(Y)O_{2-x}$; (*b*) $Zr(Ca)O_{2-x}$. Results for (*b*) are averages of all the least-squares runs. (The range of values is the size of the circle, or less.) Only one analysis was made for (*a*).

Summary

The complementary measurements of absolute X-ray diffuse scattering from disordered $Zr(Ca)O_{2-x}$ and $Zr(Y)O_{2-x}$ have produced a number of significant results. We have seen that oxygen-ion displacements occur preferentially along ⟨100⟩ directions in the fluorite lattice, but without long-range correlation. Displacement terms in the diffuse scattering, which tend to dominate in the scattering measurements, are similar for both materials, and clearly show that elastic energy is minimized by anion lattice relaxation around the oxygen vacancies (also see part I and Faber, Mueller & Cooper, 1978). Our experiments show that oxygen vacancies tend to associate with Ca^{2+} ions, *i.e.* Ca^{2+}-vacancy interactions are predominantly nearest-neighbor interactions. While this has often been suggested to interpret measurements of physical properties, this is the first experimental evidence for this. The short-range-order scattering shows features that have some resemblance to those of $CaHf_4O_9$. But several strong peaks predicted for this model are not observed. The spatial extent of ordered regions is much smaller than that proposed by Allpress & Rossell (1975) and Allpress, Rossell & Scott (1975). Further experiments on the precise structure of $CaZr_4O_9$ are needed to see if the ordered regions really resemble such a phase.

We are grateful to T. H. Etsell for lending us the crystals used in this study [which were not from the same batch used by Faber, Mueller & Cooper (1978)].

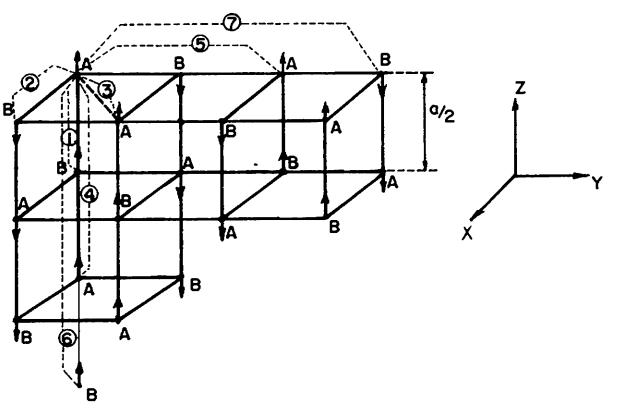

Fig. 12. Oxygen displacements in the model of the ordered stabilized zirconias (Faber, Mueller & Cooper, 1978). (*A* and *B* correspond to tet 1 and 2 in Table 1.) The numbers in the figure refer to the vectors in Table 6.

This research was supported at Northwestern University by the US Army Research Office, under Grant No. DAAG 29-76-G-0303. The X-ray work was carried out in the Long-Term X-ray Facility in Northwestern University's Materials Research Center. This facility is supported in part by NSF through Grant No. DMR-760157. One of us (JF) acknowledges the support of the Department of Energy and Argonne National Laboratory.

References

ALLPRESS, J. G. & ROSSELL, H. J. (1975). *J. Solid State Chem.* **15**, 68–78.

ALLPRESS, J. G., ROSSELL, H. J. & SCOTT, H. G. (1975). *J. Solid State Chem.* **14**, 264–273.

BATTERMAN, B. W., CHIPMAN, D. R., & DEMARCO, J. J. (1961). *Phys. Rev.* **122**, 68–74.

BORIE, B. & SPARKS, C. J. (1971). *Acta Cryst.* A**27**, 198–201.

CARTER, R. E. & ROTH, W. L. (1963). General Electric Research Report No. 63-RL-3479 M.

CARTER, R. E. & ROTH, W. L. (1968). *Electromotive Force Measurements in High-Temperature Systems*, edited by C. R. ALCOCK, pp. 125–144. New York: The Institute of Mining and Metallurgy.

CROMER, D. T. (1969). *J. Chem. Phys.* **50**, 4857–4859.

ETSELL, T. H. & FLENGAS, S. N. (1970). *Chem. Rev.* **20**, 339–376.

FABER, J. JR, MUELLER, M. H. & COOPER, B. R. (1978). *Phys. Rev. B*, **17**, 4884–4888.

GRAGG, J. E. JR, BARDHAN, P. & COHEN, J. B. (1971). *Critical Phenomena in Alloys, Magnets and Superconductors*, edited by R. E. MILLS, E. ASHER & R. JAFFEE, pp. 309–337. New York: McGraw-Hill.

HAYAKAWA, M. & COHEN, J. B. (1975). *Acta Cryst.* A**31**, 635–645.

HUANG, K. (1947). *Proc. R. Soc. London Ser. A*, **190**, 102–116.

HUDSON, B. & MOSELEY, P. T. (1976). *J. Solid State Chem.* **19**, 383–389.

HUDSON, B. & MOSELEY, P. T. (1978). *Inst. Phys. Conf. Ser.* No. 41, pp. 104–108.

International Tables for X-ray Crystallography (1974). Vol. IV. Birmingham: Kynoch Press.

KOCH, F. B. & COHEN, J. B. (1969). *Acta Cryst.* B**25**, 275–287.

MORINAGA, M. (1978). PhD Thesis, Northwestern Univ., Evanston, IL 60201.

MORINAGA, M. & COHEN, J. B. (1979). *Acta Cryst.* A**35**, 975–989.

MORINAGA, M., COHEN, J. B. & FABER, J. JR (1979). *Acta Cryst.* A**35**, 789–794.

ROTH, W. L. (1975). *Crystal Structure and Chemical Bonding in Inorganic Chemistry*, edited by C. J. M. ROOYMANS & A. RABENAN, pp. 85–102. The Netherlands: North-Holland.

SCHWARTZ, L. H. & COHEN, J. B. (1977). *Difrraction from Materials*, pp. 191–192. New York: Academic Press.

SCHWARTZ, L. H., MORRISON, L. A. & COHEN, J. B. (1963). *Adv. X-ray Anal.* **7**, 281–301.

SMITH, D. K. & Newkirk, H. W. (1965). *Acta Cryst.* **18**, 983–991.

STEELE, D. & FENDER, B. E. F. (1974). *J. Phys. C*, **7**, 1–11.

TERAUCHI, H. & COHEN, J. B. (1979). *Acta Cryst.* A**35**, 646–652.

TOKONAMI, M. (1965). *Acta Cryst.* **19**, 486.

TEUFER, G. (1962). *Acta Cryst.* **15**, 1187.

WILLIAMS, R. O. (1972). Report ORNL-4828. Oak Ridge National Laboratory, Tennessee.

WOLFF, P. M. DE (1956). *Acta Cryst.* **9**, 682–683.

Acta Cryst. (1980). A**36**, 530–535

Theory of Piezo-Optic Birefringence in Mixed Crystals of Equimolar Concentration with NaCl Structure

BY G. S. KUMAR, R. ETHIRAJ AND V. G. KRISHNA MURTY

Department of Physics, Osmania University, Hyderabad 500 007, *India*

(*Received* 24 *August* 1979; *accepted* 24 *December* 1979)

Abstract

Following the theoretical approach of Bansigir & Iyengar [*Acta Cryst.* (1961), **14**, 670–674], an expression for $p_{11} - p_{12}$ is developed for a mixed crystal of KCl–KBr with equimolar concentration. It was assumed that among the six nearest neighbours of the K^+ ion, three are Cl^- and the other three Br^-, and that each K^+ is accompanied by Cl^- and Br^- on either side in all three principal directions. The expression $p_{11} - p_{12}$ is used to evaluate the polarizabilities, reversal wavelength, ratio and absolute values of strain–optical constants p_{11} and p_{12}.

Introduction

Some years ago, an improved theory of piezo-optic birefringence in cubic crystals of NaCl structure was

0567-7394/80/040530-06$01.00